

Regional Total Electron Content Map Generation based on Compressive Sensing

Cansu Sunu, Cenk Toker

Abstract

Ionosphere has an important role in long distance HF communications, satellite communications and global navigation systems. Ionosphere is a plasma medium which arises due to solar and cosmic radiation, and the amount of ionization is highly time and location dependent. Eventually, the current state of the ionosphere should be continuously monitored with high accuracy. Total Electron Content (TEC) maps are being used to investigate the state of the ionosphere. There are online services which provide TEC maps, however they mostly have low spatial and temporal resolution and the techniques used for generating these maps are generally not accessible.

TEC maps can also be generated from GNSS/GPS based Continuously Operating Receiver Stations (CORS) network measurements. Unfortunately, the GNSS/GPS receiver networks are not dense enough to form a map directly. Therefore, an algorithm should be used to estimate the TEC values at coordinates without a receiver. Based on the observation that TEC maps possess a high degree of sparsity, we propose a modified compressive sensing technique for generating regional TEC maps by using the sparse dataset obtained from a CORS network.

We evaluate the performance of the proposed technique both over synthetically generated TEC maps which mimic the common characteristics of the ionosphere, and also over actual measurements taken over the Turkish National Permanent GPS Network (TNPNG) Active. Our analysis reveals that the proposed technique can produce TEC maps with high accuracy and resolution. We also demonstrate the superiority of our technique over other TEC map generation techniques found in the literature.

Index Terms

Compressive Sensing (CS), Total Electron Content (TEC), Ionosphere, Kriging, Two Dimensional Discrete Cosine Transform (2D-DCT).

I. INTRODUCTION

IONOSPHERE, located at an altitude of between 90 km and 1100 km above the Earth, is a plasma medium ionized by high energy solar and cosmic radiations. Ionosphere plays an important role in long distance communications, satellite communications and global navigation systems since all these signals pass through the ionosphere as the propagation medium.

Space Weather (SW) phenomena such as solar flares, and ionospheric storms strongly affect the structure of the ionosphere. The performance of the systems mentioned above can significantly be deteriorated and even sometimes they cannot be used temporally due to ionospheric disturbances. The ionosphere varies considerably with time, location, activities of sun, and geomagnetic storms, hence the structural variations of the ionosphere have to be observed and tracked continuously [1]. The key parameter used to express the ionospheric structure is the Total Electron Content (TEC). TEC, which is defined as the total number of electrons contained in a hypothetical semi-infinite cylinder with a base area of 1 m^2 positioned on the ground and aligned in the vertical direction. Unit of TEC is TECU and 1 TECU is 10^{16} electrons/ m^2 .

TEC is not directly measurable, but its value is estimated by indirect measurements made using ground- or space-based measurement systems. Ground-based systems are ionosondes, backscatter radars, and noncoherent backscatter radars etc. Space-based systems depend on systems such as Global Positioning System (GPS), GLONASS, and TOPEX/Poseidon. Since GPS is a global system and there are several Continuously Operating Receiver Stations (CORS) networks composed of hundreds of GPS receivers deployed both globally and also regionally such as International GNSS Stations (IGS), Regional Reference Frame Sub-Commission for Europe (EUREF), Turkish National Permanent GPS Network (TNPNG) Active, etc., TEC measurements from GPS signals is a widely used technique, [2]–[5].

Temporal and spatial variability of the ionosphere can be represented by the temporal and spatial correlation of the electron density of the ionosphere. Quiet and disturbed days are investigated in [6], and it is shown that temporal correlation varies from 3 to 25 mins for quiet days and from 3 to 15 mins for disturbed days [7]. Shorter correlation time and correlation distance values are indications of high variability in the ionosphere. The spatial and temporal behaviour of the ionosphere can be effectively analysed using two dimensional TEC maps [8]–[12]. In [8], global 1° (lat) \times 1° (lon) TEC maps are analysed using 2-Dimensional Discrete Cosine Transform (2D-DCT), where it is shown that the maps can be represented by using a small number of 2D-DCT coefficients. Specifically, it was shown that 90% of the energy content of the DCT coefficients of a TEC map is contained within the largest 20 coefficients of the transform of a $180 \times 360 = 64800$ pixel TEC map. This observation demonstrates the high sparsity level of TEC maps in the DCT domain. Similar results on the sparsity level of the TEC maps for the mid latitude region are also shown in [1].

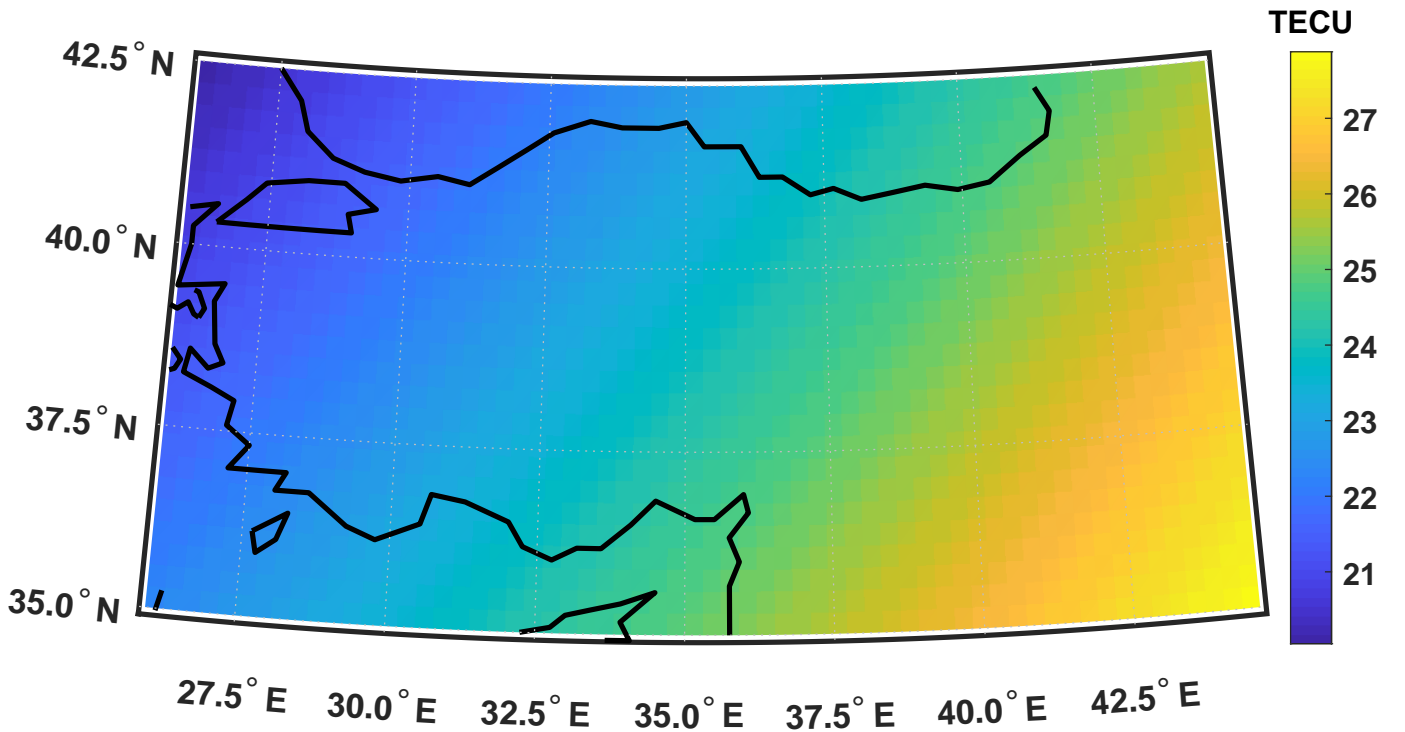


Fig. 1. Synthetic map 1: Linear trend. Represents the dawn of a quiet day.

Compressive Sensing (CS) is a method successfully applied to signals which are highly sparse in a certain transform domain. In contrast to the conventional sampling theorem, where uniformly spaced samples of the signal are required with a sampling frequency of at least twice the bandwidth of the signal of concern, a much smaller number of samples with non-uniform (possibly random) spacing are adequate to recover the original signal from these sparse samples in CS, given that the signal is highly sparse in a transform domain. Signal recovery is done by using optimization problems or iterative algorithms [13]–[15]. The concept and applications of compressive sensing are reviewed in [16] in detail. Some of the major application areas of CS are radar imaging systems, biomedical applications, pattern recognition, and communications networks [17]–[21]. In this paper, the compressive sensing technique is applied to the regional TEC map estimation based on the sparse nature of the TEC maps. Application of compressive sensing to the TEC map generation presented in this paper is a novel technique.

TEC maps are being published online by several research/government organizations through their webpages [23]–[27]. However these maps have low spatial and temporal resolution (e.g. NASA-JPL (IARS) [23] produces 2.5° (lat) \times 5° (lon) maps at each 5 minutes, DLR (IMPC) [24] produces 2.5° (lat) \times 5° (lon) global and 2° (lat) \times 2° (lon) regional (Europe) maps at an update rate of 15 minutes, SWS [26] produces global/regional maps at each 15 minutes, UNIBE (CODE-GIM) [27] maps are produced at a resolution of 2.5° (lat) \times 5° (lon) and 2 hours, where the near real-time maps are produced through a “rapid” process and final maps are provided a couple of days later. Moreover, the processes being used to produce these maps are not open to the public access.

Eventually, for the purpose of real-time monitoring of the ionosphere, observing ionospheric anomalies such as travelling ionospheric disturbances (TIDs), and making real-time corrections for GNSS based navigation systems, the services mentioned above may not be adequate. In this paper, we propose a technique which produces TEC maps with a spatial resolution better than 0.5° (lat) \times 0.5° (lon) and a temporal resolution of as low as 30 sec.s. Moreover, TEC maps can be generated as soon as the GNSS/GPS data is available, making our technique “real time”.

An alternative to our proposed technique is based on Kriging [34], [35]. In this technique, TEC measurements from GNSS receivers are used to construct the TEC map, however, the reconstruction performance deteriorates with increasing resolution, and artifacts appear, especially in regions where extrapolation needs to be done. Our technique is superior to Kriging both in the sense of improved resolution and also reconstruction performance, as will be compared in this paper.

Section II introduces the system model, and discusses 2D-DCT domain representation of a TEC map. Sparsity levels of synthetically generated maps, and the optimization problem which is used to recover the map from a set of samples are also provided in Section II. In Section III, the performance of the proposed technique on synthetically generated maps in the sense of normalized error energy is analysed. In Section IV, map estimations are made using GPS-TEC data from Turkish National Permanent GPS Network (TNPNG) Active and results are compared with the Kriging method [34], [35]. Finally, Section V concludes the paper.

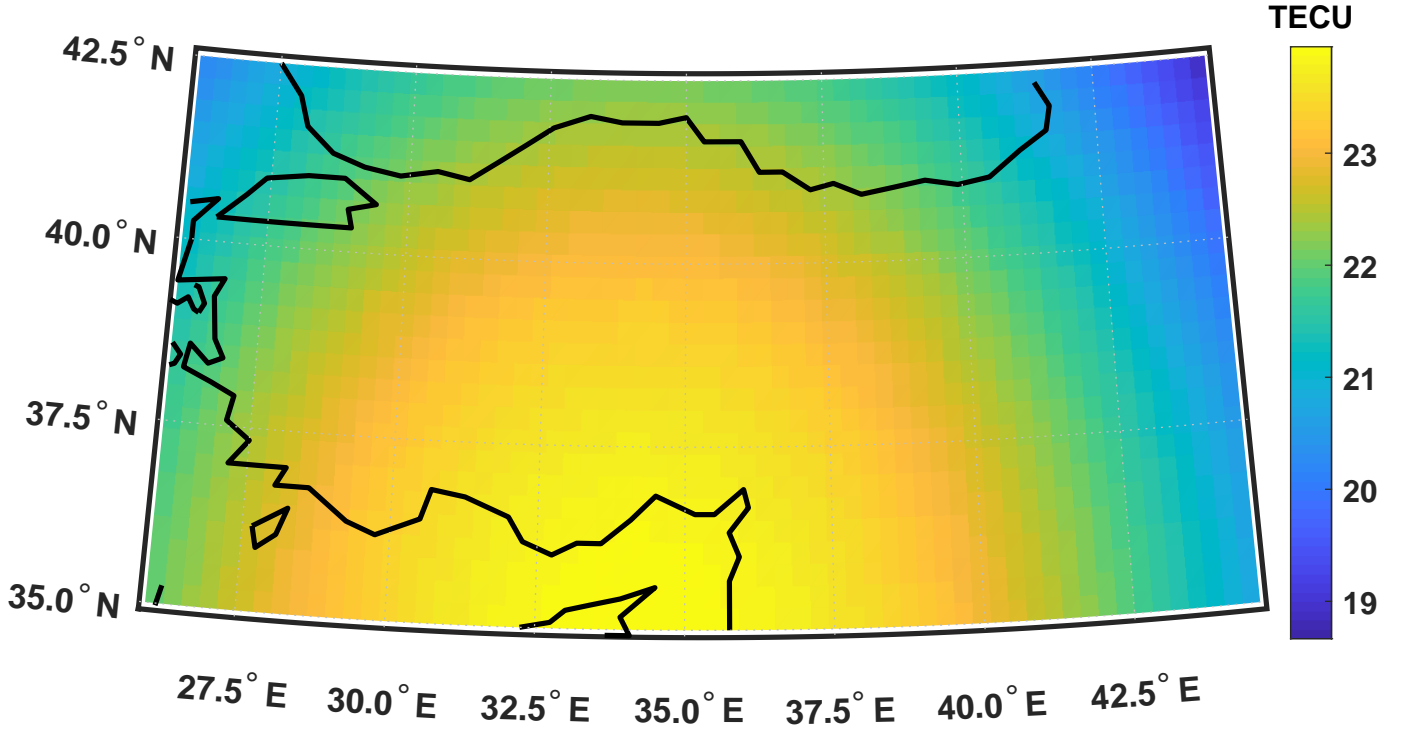


Fig. 2. Synthetic map 2: Quadratic trend. Represents the midday of a quiet day.

II. SYSTEM MODEL AND PROBLEM FORMULATION

In this section, we construct the mathematical basis of the problem and provide an optimization problem formulation for the reconstruction of the TEC maps.

A. Notation

Let a TEC map of a “rectangular” region between coordinates ϕ_{\min} and ϕ_{\max} in latitude and λ_{\min} and λ_{\max} in longitude (following the geodetic coordinate system convention) at a given time be represented by a $P \times Q$ matrix \mathbf{U}

$$\mathbf{U} = \begin{bmatrix} U_{0,0} & U_{0,1} & \cdots & U_{0,Q-1} \\ U_{1,0} & U_{1,1} & \cdots & U_{1,Q-1} \\ \vdots & \vdots & \ddots & \vdots \\ U_{P-1,0} & U_{P-1,1} & \cdots & U_{P-1,Q-1} \end{bmatrix}. \quad (1)$$

If a grid structure on the map is visualized with resolution $\Delta\phi$ in latitude and $\Delta\lambda$ in longitude, the real-valued scalar $U_{p,q}$ gives the TEC value at the coordinate $(\phi_{\min} + p\Delta\phi, \lambda_{\min} + q\Delta\lambda)$. We assume that the lower-left pixel of the map is the origin.

Let the orthonormal bases for 2D-DCT be defined as

$$D_{k,l}(p,q) = \alpha_k \alpha_l \cos\left(\frac{\pi(2p+1)k}{2P}\right) \cos\left(\frac{\pi(2q+1)l}{2Q}\right) \quad (2)$$

where α_k and α_l are normalization factors and defined as $\alpha_k = \sqrt{\frac{1}{P}}$, if $k = 0$ and $\alpha_k = \sqrt{\frac{2}{P}}$, if $k = 1, \dots, P-1$, and $\alpha_l = \sqrt{\frac{1}{Q}}$, if $l = 0$ and $\alpha_l = \sqrt{\frac{2}{Q}}$, if $l = 1, \dots, Q-1$, respectively.

Using (2), each entry of the matrix \mathbf{U} in (1) can be represented in terms of the 2D-DCT coefficients, $S_{k,l}$, as

$$U_{p,q} = \sum_{k=0}^{P-1} \sum_{l=0}^{Q-1} S_{k,l} D_{k,l}(p,q). \quad (3)$$

The $N \times 1$ map vector is defined as

$$\begin{aligned} \mathbf{u} &= \text{vec}(\mathbf{U}) \\ &= [u_0 \ u_1 \ u_2 \ \cdots \ u_{N-1}]^T \end{aligned} \quad (4)$$

where $u_n = U_{p,q}$ with $n = Pq + p$ and $N = PQ$. Similarly, the $N \times 1$ 2D-DCT coefficients vector is defined as

$$\mathbf{s} = [s_0 \ s_1 \ s_2 \ \cdots \ s_{N-1}]^T \quad (5)$$

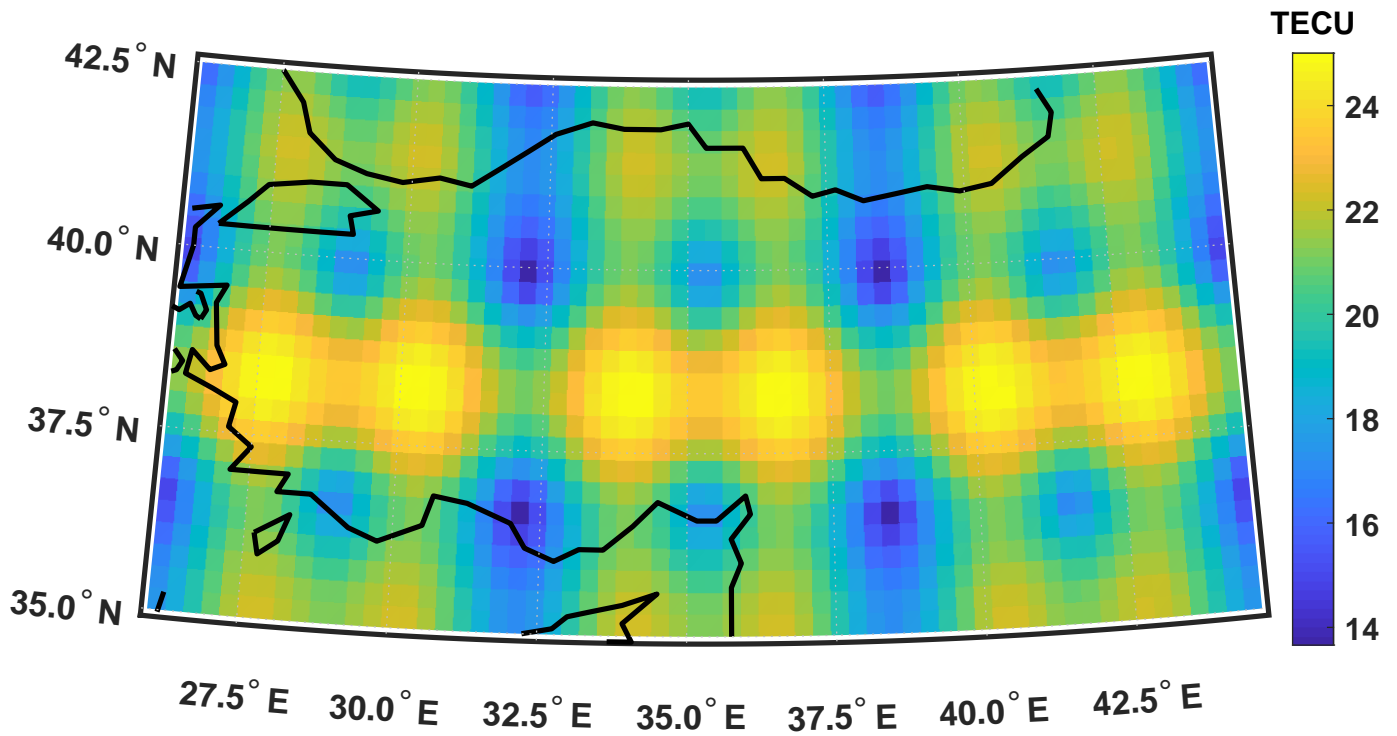
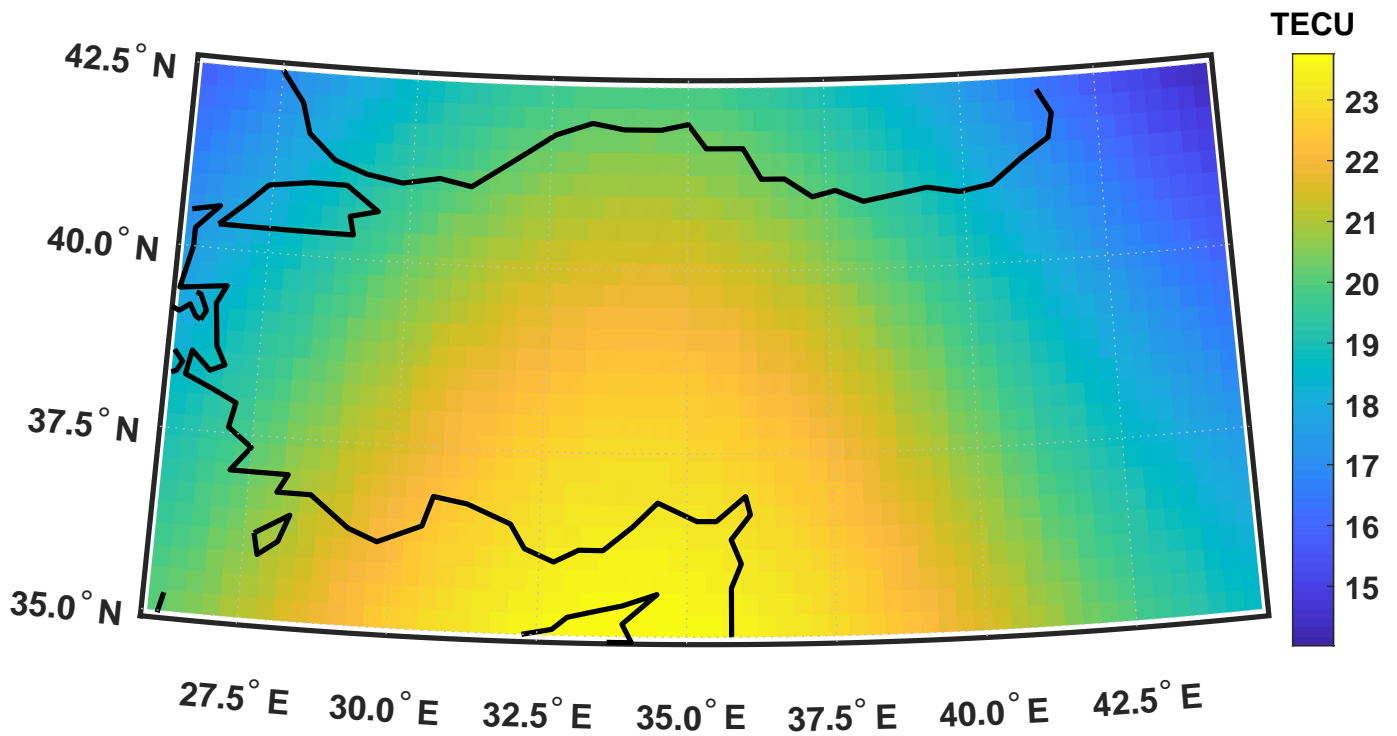


Fig. 4. Synthetic map 4: Mixture of Gaussian trend and sinusoidal disturbance. Represents the midday of a disturbed day.

where $s_t = S_{k,l}$ with $t = Pl + k$. Using (3)-(5), we can write

$$\mathbf{u} = \mathbf{D}\mathbf{s} \quad (6)$$

where \mathbf{D} is an $N \times N$ transform matrix and given by

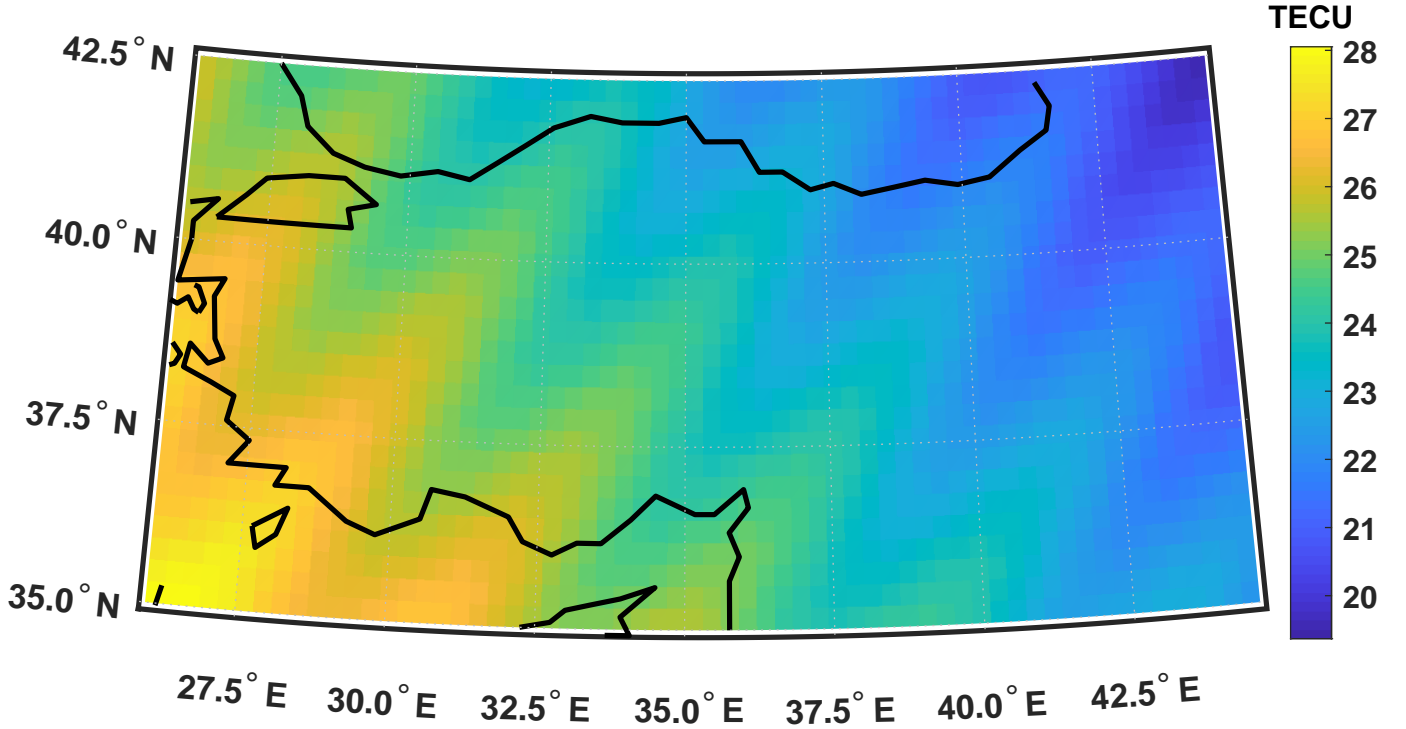


Fig. 5. Synthetic map 5: Mixture of linear trend and sinusoidal disturbance. Represents the dusk of a disturbed day.

TABLE I
MATHEMATICAL REPRESENTATION OF SYNTHETIC MAPS (SMS)

SM 1	$\text{TEC}(\phi, \lambda) = 25 - 0.3\phi + 0.3\lambda$
SM 2	$\text{TEC}(\phi, \lambda) = 25 - 0.3(\phi - 34)^2 + 0.3(\lambda - 35)^2$
SM 3	$\text{TEC}(\phi, \lambda) = 20 + 5e^{-\left(\frac{\phi-34}{10}\right)^2 - \left(\frac{\lambda-35}{7}\right)^2}$
SM 4	$\text{TEC}(\phi, \lambda) = 21 + 6\sqrt{\cos^2(\phi - 35) + \sin^2(\lambda - 32)}$ $- 6e^{0.25\{\cos(\phi-35)+\cos(\lambda-32)\}}$
SM 5	$\text{TEC}(\phi, \lambda) = 46 - 0.3\phi - 0.3\lambda + 0.5 \cos(1.5(\lambda - \phi))$

TABLE II
SPARSITY LEVELS OF SYNTHETIC MAPS (SMS)

SM 1	SM 2	SM 3	SM 4	SM 5
3	7	6	21	11

$$\mathbf{D} = \begin{bmatrix} \tilde{D}_0(0) & \cdots & \tilde{D}_t(0) & \cdots & \tilde{D}_{N-1}(0) \\ \tilde{D}_0(1) & \cdots & \tilde{D}_t(1) & \cdots & \tilde{D}_{N-1}(1) \\ \vdots & \vdots & \vdots & \vdots & \vdots \\ \tilde{D}_0(N-1) & \cdots & \tilde{D}_t(N-1) & \cdots & \tilde{D}_{N-1}(N-1) \end{bmatrix} \quad (7)$$

where $\tilde{D}_t(n) = D_{k,t}(p, q)$ with $n = Pq + p$ and $t = Pl + k$.

B. TEC Map Generation Based on Compressive Sensing

Although a TEC map (the matrix \mathbf{U}) is composed of $N = PQ$ pixels, assume that only M of them are available as measured values, i.e. $M \leq N$. Let the pixels with measurements be represented by the set

$$\mathcal{O} = \{(p_m, q_m) \mid p_m \in [0, P-1], q_m \in [0, Q-1]\} \quad (8)$$

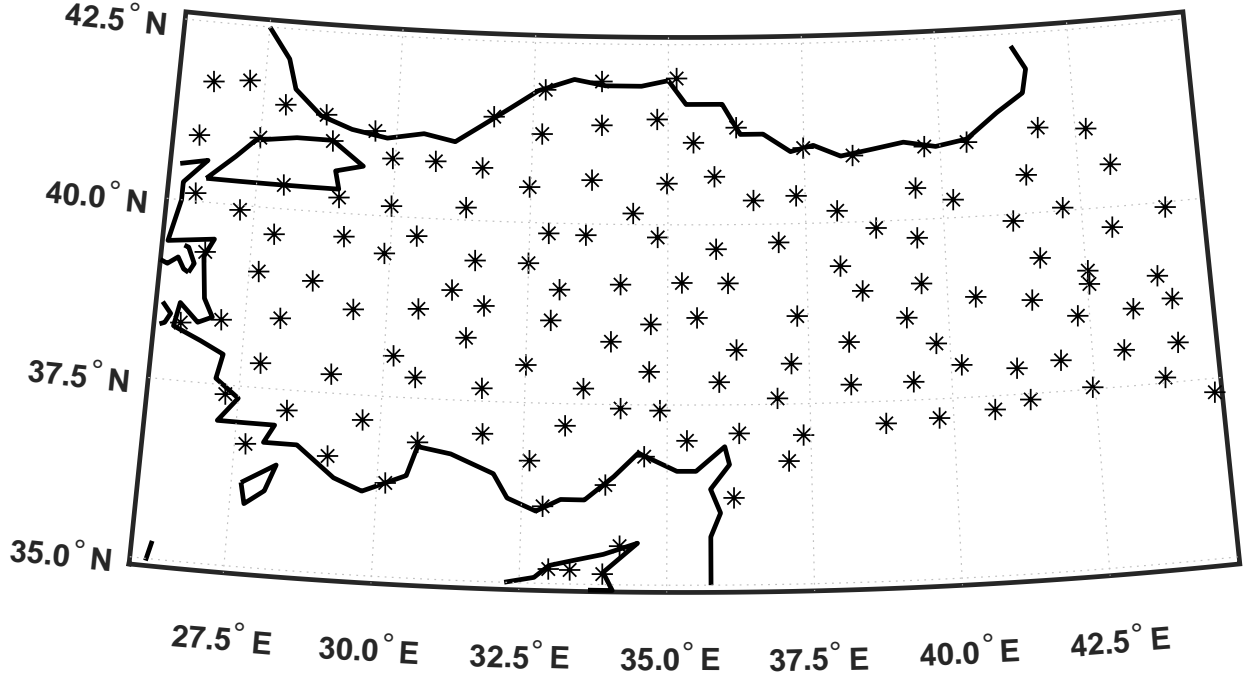


Fig. 6. Reference station network of TNPNG-Active

where $m = 0, \dots, M-1$ and $p_m, q_m \in \mathbb{Z}$. Let the measurements be stacked in an $M \times 1$ vector as

$$\begin{aligned}
 \mathbf{b} &= \begin{bmatrix} b_0^{(i_0)} \\ \vdots \\ b_m^{(i_m)} \\ \vdots \\ b_{M-1}^{(i_{M-1})} \end{bmatrix} = \begin{bmatrix} \mathbf{e}_{i_0}^T \mathbf{u} \\ \vdots \\ \mathbf{e}_{i_m}^T \mathbf{u} \\ \vdots \\ \mathbf{e}_{i_{M-1}}^T \mathbf{u} \end{bmatrix} \\
 &= [\mathbf{e}_{i_0} \quad \mathbf{e}_{i_1} \quad \cdots \quad \mathbf{e}_{i_{M-1}}]^T \mathbf{u} \\
 &= \mathbf{M} \mathbf{u}
 \end{aligned} \tag{9}$$

where $i_m = Pq_m + p_m$, and \mathbf{e}_{i_m} denotes the $N \times 1$ vector with a 1 in the i_m -th entry and 0's elsewhere, and \mathbf{M} is the $M \times N$ measurement matrix. Substituting (6) into (9) yields

$$\mathbf{b} = \mathbf{A} \mathbf{s} \tag{10}$$

where the $M \times N$ matrix $\mathbf{A} = \mathbf{M} \mathbf{D}$ is called the sensing matrix.

The conventional CS formulation¹, when used with the DCT basis, does not differentiate between low frequency and high frequency components. However, due to physical limitations, the TEC value cannot change abruptly in the spatial domain, i.e. a TEC map has a lowpass nature, as it is demonstrated in [7].

To incorporate this lowpass characteristic to the problem, we propose a two part cost function as the following

$$\begin{aligned}
 \arg \min_{\mathbf{s}} \quad & \|\mathbf{W} \mathbf{s}\|_1 + \gamma f(\mathbf{D} \mathbf{s}) \\
 \text{subject to} \quad & \frac{\|\mathbf{A} \mathbf{s} - \mathbf{b}\|_2^2}{\|\mathbf{b}\|_2^2} \leq \epsilon
 \end{aligned} \tag{11}$$

where $\mathbf{W} = \text{diag}(1/w_0, 1/w_1, \dots, 1/w_{N-1})$ is a square diagonal weighting matrix such that

$$w_i = \frac{1}{1 + \frac{k^2 + l^2}{\sigma^2}}, \quad \text{for } i = Pl + k \tag{12}$$

where the weights w_i represent the coefficients of a first order Butterworth lowpass filter, and σ is the cut-off wave number in both dimensions. Furthermore, we use a regularization function, $f(\cdot)$, defined as

$$f(\mathbf{u}) = \|\nabla_x \mathbf{u}\|_2^2 + \|\nabla_y \mathbf{u}\|_2^2 \tag{13}$$

¹In a conventional CS formulation, the optimization problem would be $\arg \min_{\mathbf{x}} \|\mathbf{x}\|_1$, subject to $\|\mathbf{A} \mathbf{x} - \mathbf{b}\|_2^2 < \epsilon$, [15], where the cost function aims at minimizing the sparsity level of the problem in the transform domain (the actual formulation contains $\|\cdot\|_0$ where $\|\cdot\|_1$ is used as a mathematically tractable approximation of $\|\cdot\|_0$, [14]) and the constraint guarantees to limit the reconstruction error below a threshold level ϵ .

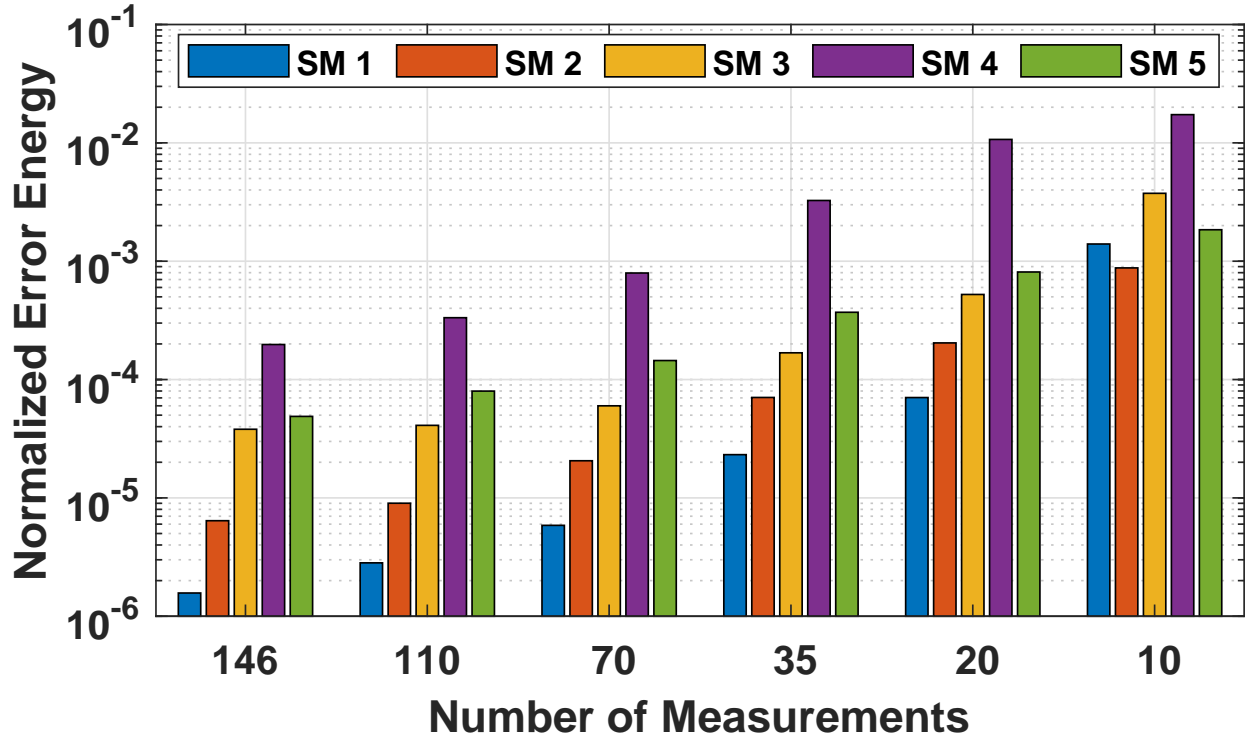


Fig. 7. Effect of number of observation to the performance for each synthetic maps

to limit the variation in both spatial dimensions, where ∇_x and ∇_y are the gradient operators in x- and y-direction, respectively. We use CVX [22] as a solver for the problem in (11).

III. PERFORMANCE EVALUATION OF THE PROPOSED TECHNIQUE

In this section, we will analyze the performance of the proposed CS based TEC map estimation technique given in (11). There are certain patterns of the ionosphere depending on both the time of the day, such as dawn, midday, dusk, and also the state of the ionosphere, such as those at a quiet day and at a disturbed day. Due to the time varying and random characteristic of the ionosphere, it might be difficult to observe these patterns explicitly. Therefore, we will first investigate the performance of our technique on synthetically generated maps which mimic the typical states of the ionosphere.

A. Performance Evaluation over Synthetic Maps

As a first set of performance evaluation, we have generated several synthetic TEC maps representing the typical patterns of the dawn (Fig. 1) and the midday (Figs. 2 and 3) of a quiet day, and the midday (Fig. 4) and the dusk (Fig. 5) of a disturbed day. Expressions for generating the maps are given in Table I. Also, Table II demonstrates the sparsity level of the TEC maps in Fig. 1 to 5. Noting that there are $PQ = 1638$ pixels in each map, it is clear that the maps are highly sparse, justifying the suitability of CS for the reconstruction of TEC maps from few measurements.

Fig. 6 shows the coordinates of the 146 fixed GPS reference stations which constitute the TNPNGN-Active CORS Network. We assess the performance of the proposed technique by taking samples from the synthetic maps at these coordinates only². Note the considerable amount of extrapolation done close to the boundaries of the map. The metric that we use for performance evaluation is the normalized error energy defined by

$$\mathcal{E}_p = \frac{\|\mathbf{u} - \hat{\mathbf{u}}\|_2^2}{\|\mathbf{u}\|_2^2} \quad (14)$$

where \mathbf{u} is the synthetic map vector defined in (1) and (4), and $\hat{\mathbf{u}}$ is the reconstructed map vector given by $\hat{\mathbf{u}} = \mathbf{D}\mathbf{s}$, and \mathbf{s} is the solution of the problem in (11).

The performance of the algorithm depends on the values of the parameters σ and γ given in (11) and (12). Examining over a wide range of values of σ and γ , $(\sigma, \gamma) = (5, 1)$ is found to be a good choice which yields relatively low reconstruction error for all synthetic maps. Our numerical analysis has revealed that this set results in a normalized error energy of 1.9×10^{-4} as the worst case for SM4 and lower normalized error energy values for the other synthetic maps.

²We consider a resolution of 0.3° (lat) \times 0.3° (lon). If the actual coordinates of a GPS receiver does not match a map grid point, we assign the measurement value to the nearest grid point. Although there may be other assignment methods, our approach is acceptable due to the low-pass characteristic of the TEC map and for a dense-enough grid structure

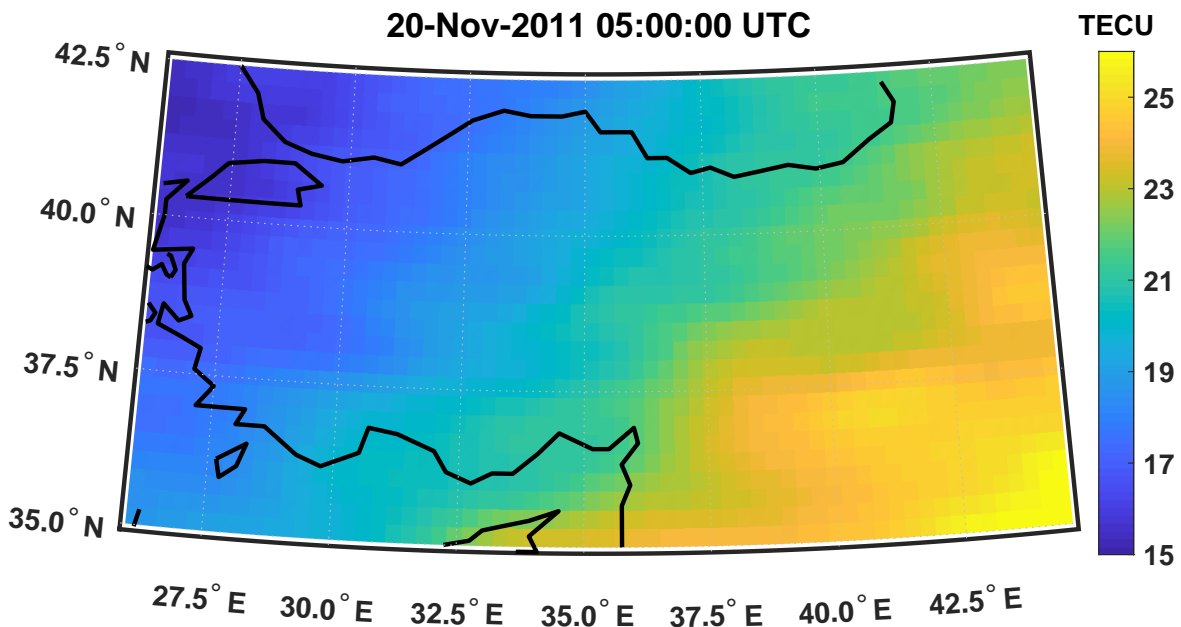


Fig. 8 Estimated map at 05:00 UTC on 20 Nov 2011, Compressive Sensing

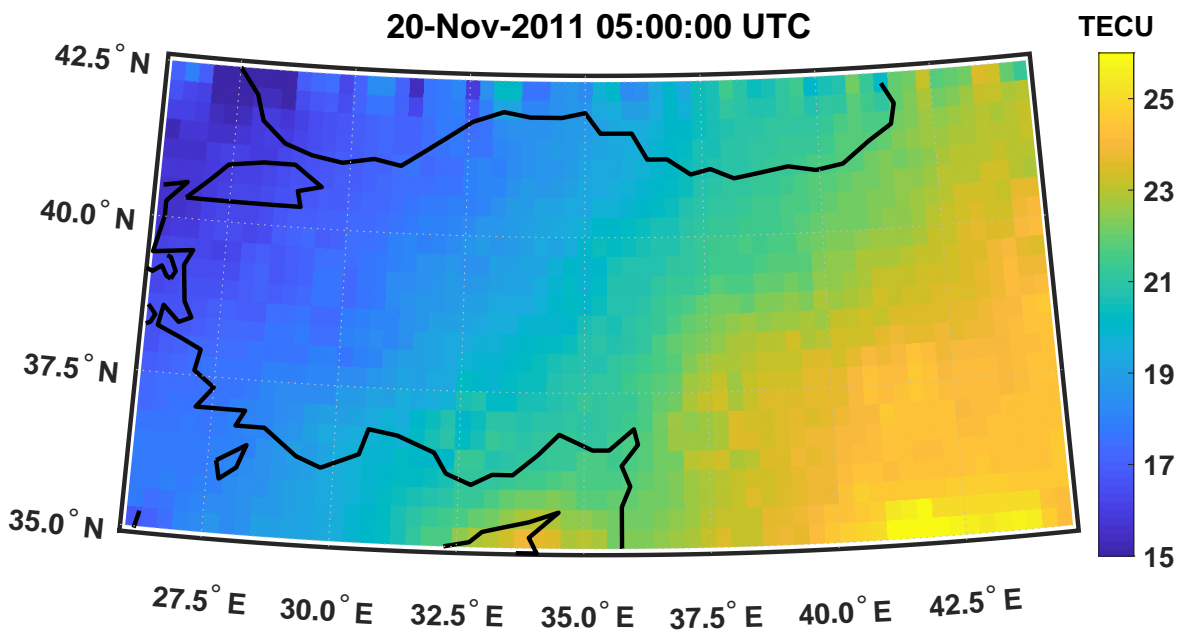


Fig. 9. Estimated map at 05:00 UTC on 20 Nov 2011, Kriging

An important parameter that has effect on the performance of CS is the number of samples taken. Considering the number of GPS receivers in the TNPNGN-Active network, we assume that at most 146 samples (measurements) can be taken for a TEC map. However, due to several reasons in practice, only a subset of these receivers may be available. Fig. 7 examines the performance of the proposed technique for various number of measurements. For each synthetic map scenario, and each number of measurements, 100 different realizations are conducted with randomly chosen samples from the full set of 146 samples, and the normalized error energy metric is averaged over these realizations.

Fig. 7 demonstrates that even if half of the samples (i.e. 70 samples) are available, the normalized error energy is below 4×10^{-4} for all synthetic maps. Considering the sparsity levels in Table II, this is coherent with the general observation that the number of samples approximately equal to five times the sparsity level is adequate for a good reconstruction [14]–[16].

B. Performance Evaluation over Measurement Data

By using the RINEX measurements of the GPS receivers at the TNPNGN-Active network (Fig. 6), we first calculate the TEC estimates at the sampling points in the local zenith direction by using the IONOLAB-TEC algorithm [2], [3], [28], [29], for 25 June 2011 16:40 UTC and 20 November 2011 05:00 UTC. IONOLAB-TEC is a state-of-the-art signal processing technique

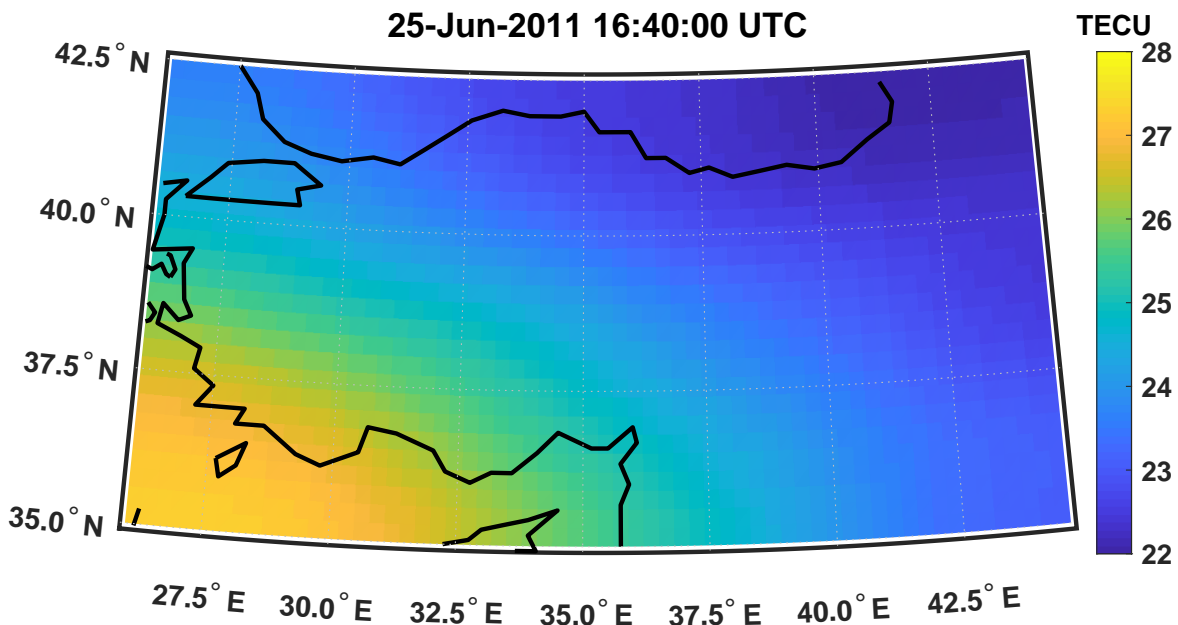


Fig. 10. Estimated map at 16:40 UTC on 25 Jun 2011, Compressive Sensing

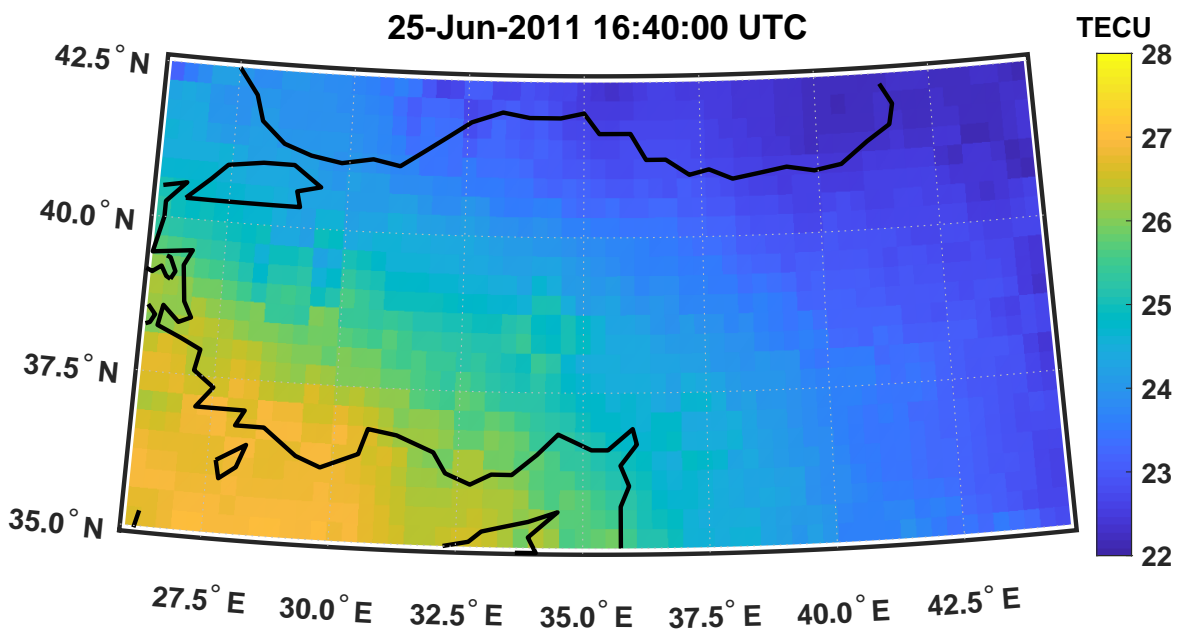


Fig. 11. Estimated map at 16:40 UTC on 25 Jun 2011, Kriging

that calculates the TEC value in the local zenith direction at a specific location (e.g. a CORS GPS receiver) by combining IONOLAB-BIAS and Vertical TEC (VTEC) for each satellite in the least square sense by employing a weighting function. VTEC is the total number of electrons in the local zenith direction obtained from Slant TEC (STEC) by the use of a "mapping function". The number of available measurements are respectively 122 and 124 out of the 146 sampling points for the epochs mentioned above.

TEC maps generated by the proposed CS based technique are given in Figs. 8 and 10. We evaluate the performance of the proposed technique in two ways.

First, a number of measurements are randomly selected and kept out of the dataset that we use for generating the TEC maps with the proposed algorithm. Next, these measurements are compared with the estimates at the same coordinates of the TEC map in terms of the normalized error energy given in (14). We repeat this procedure 1000 times and take the average of the normalized error energy. The results are provided in Figs. 12 and 13 for different number of cross-check points. It can be seen that with 10 to 30 cross-check points, the error energy is below 1.85×10^{-4} for the epoch in Fig. 13 and below 5.6×10^{-4} for the epoch in Fig. 12 which are reasonably low, justifying the excellent performance of the proposed algorithm. Note that, as we increase the number of cross-check points, the performance deteriorates since the number of measurements included in

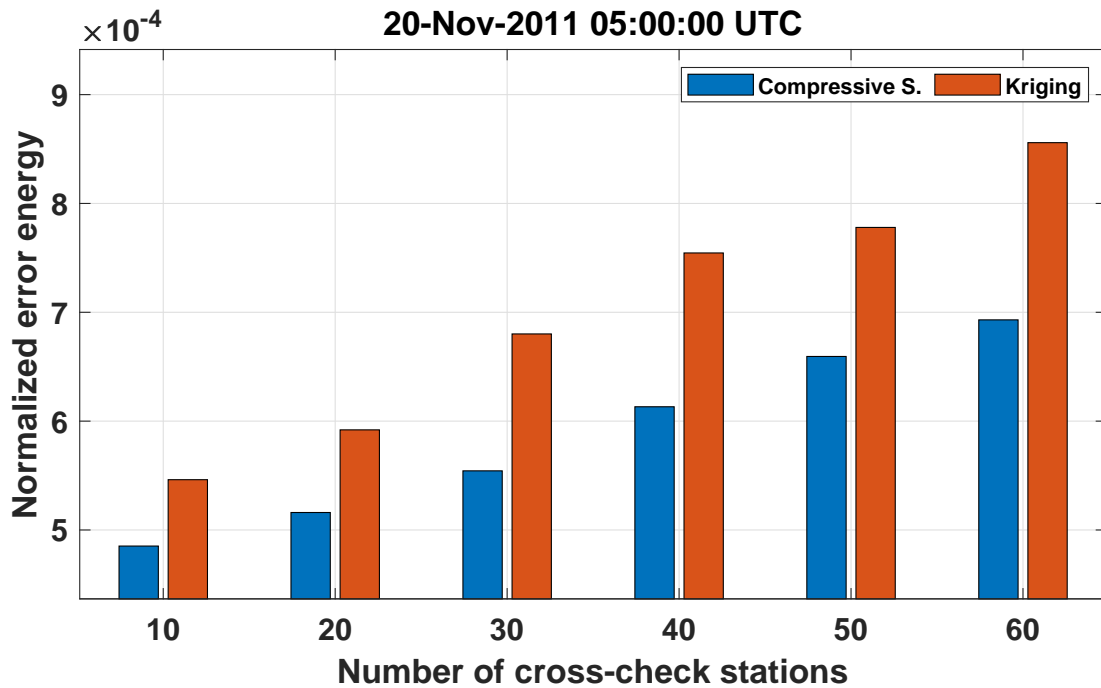


Fig. 12. Cross check at 05:00 UTC on 20 Nov 2011

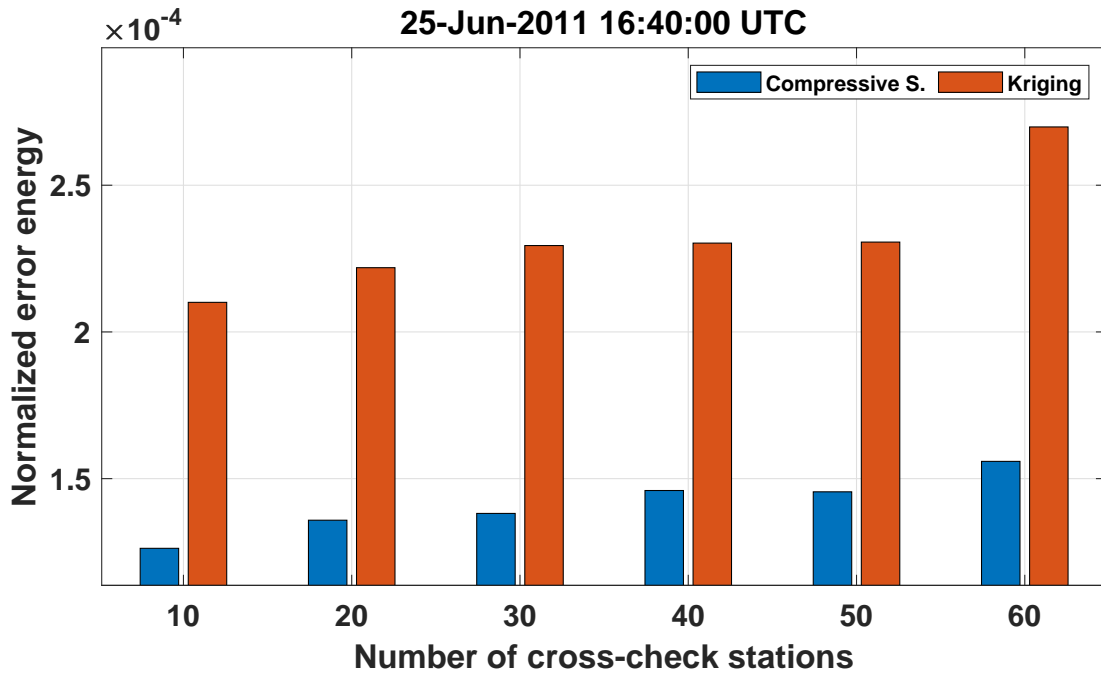


Fig. 13. Cross check at 16:40 UTC on 25 Jun 2011

the dataset of the algorithm decreases as it was demonstrated in Fig. 7 for the synthetic maps.

Kriging, interpolation with spherical harmonics, thin plate spline interpolation and neural networks [30]–[35] are some of the methods used for TEC map generation in the related literature. For a second evaluation, we compare the performance of the proposed technique with the state-of-the-art technique based on Kriging [33], [35]. Kriging algorithm uses inverse distance weighting to increase the number of samples in the dataset then generates TEC map by using ordinary Kriging with isotropic semivariogram. TEC maps generated by Kriging with the same dataset that we use to generate the TEC maps with our proposed technique, are shown in Figs. 9 and 11. Artificial fluctuations can be clearly seen by comparing Figs. 9-11 and 8-10, especially for the regions close to the edges of the map. Such fluctuations are not physically possible due to the nature of the ionosphere.

We also conducted a cross-check test similar to that is done for the proposed CS technique. Cross-check results for Kriging are also provided in Figs. 12 and 13. It can be concluded that the normalized error energy performance of our technique is better than that of Kriging, justifying the superiority of our technique.

IV. CONCLUSION

In this paper, a modified compressive sensing technique is proposed for generating regional TEC maps by using a dataset obtained from a CORS network. The algorithm is based on the observation that TEC maps have a lowpass structure, and they can be highly sparse in the 2D-DCT domain.

To examine the performance of the proposed technique, we use synthetically generated TEC maps which mimic some of the common characteristics of the ionosphere. Several parameters of the technique, such as the weights of the algorithm, number of measurements required, are tuned over these maps. Analysis has revealed that the normalized-error-energy can be as low as 10^{-5} to 10^{-4} .

We further use actual TNPNG-Active CORS network measurement data to assess the performance of the proposed technique. A cross-check based method is adopted and it is shown that the proposed technique can estimate the TEC map with high fidelity, even for a very high resolution of 0.5° (lat) \times 0.5° (lon). We also compare the CS based technique with the state-of-the-art in the literature, a Kriging based algorithm. The proposed technique outperforms the Kriging based algorithm both in terms of normalized-error-energy and yields better perception and also fits better to the physical behaviour of the ionosphere.

Our analysis with measurement data also revealed that approximately 100 GPS-CORS measurements are adequate to map a region of 7.5° (lat) \times 20° (lon) at a resolution of 0.5° (lat) \times 0.5° (lon), i.e. 1638 pixels.

REFERENCES

- [1] B. Yilmaz and C. Toker, "Spatial-Spectral Analysis of Ionospheric TEC Maps," 2017 25th Signal Processing and Communications Applications Conference (SIU), 2017.
- [2] F. Arkan, C. B. Erol, and O. Arkan, "Regularized Estimation of Vertical Total Electron Content from Global Positioning System Data", J. Geophys. Res., 108, 1469, 2003.
- [3] F. Arkan, C.B. Erol and O. Arikani, "Regularized Estimation of VTEC from GPS Data for A Desired Time Period", Radio Science, 39, 2004.
- [4] C.B. Erol and F. Arkan, "Statistical Analysis of The Ionosphere using GPS Signals", Journal of Electromagnetic Waves and Applications, 2005.
- [5] F. Arkan and O. Arkan, "Adaptive Tracking of Narrowband HF Channel Response", Radio Science, 2003.
- [6] I. Sayn, F. Arkan and K. E. Akdoan, "Optimum Temporal Update Periods for Regional Ionosphere Monitoring," Radio Science, 2010.
- [7] S. D. Yenen, U. Sezen and F. Arikani, "Modelling the Spatial-Temporal Variability of The Ionosphere over Turkey Using A GPS Network," 2017 XXXIInd General Assembly and Scientific Symposium of the International Union of Radio Science (URSI GASS), 2017.
- [8] C. Sunu and C. Toker, "Sparse 2D-DCT Reconstruction of Total Electron Content Maps," 2019 9th International Conference on Recent Advances in Space Technologies (RAST), Istanbul, Turkey, 2019.
- [9] A. J. Mannucci, B. D. Wilson, D. N. Yuan, C. H. Ho, U. J. Lindqwister and T. F. Runge, "A Global Mapping Technique for GPS-Derived Ionospheric Total Electron Content Measurements," Radio Science, 1998.
- [10] B. Zhao, W. Wan, L. Liu, and T. Mao, "Morphology in The Total Electron Content Under Geomagnetic Disturbed Conditions: Results from Global Ionosphere Maps" Annales Geophysicae, 25 (7), 1555-1568, 2007.
- [11] L. Liu, W. Wan, B. Ning, and M.-L. Zhang, "Climatology of The Mean Total Electron Content Derived from GPS Global Ionospheric Maps," Journal of Geophysical Research, 114, A06308, 2009.
- [12] A. Meza, M. P. Natali, and L. I. Fernandez, "Analysis of The Winter and Semiannual Ionospheric Anomalies in 19992009 Based on GPS Global International GNSS Service Maps," Journal of Geophysical Research, 117, A01319, 2012.
- [13] X. Wang and L. Zhang, "Compressed Sensing Image Reconstruction Algorithm Based on Regional Segmentation," 7th International Congress on Image and Signal Processing, 2014.
- [14] Y. C. Eldar and G. Kutyniok, "Compressed Sensing: Theory and Applications," Cambridge University Press, 2012.
- [15] E. Candes. "Compressive Sampling," Proceedings of the International Congress of Mathematicians, Madrid, Spain, Aug. 2006.
- [16] M. Rani, S. B. Dhok and R. B. Deshmukh, "A Systematic Review of Compressive Sensing: Concepts, Implementations and Applications," in IEEE Access, vol. 6, pp. 4875-4894, 2018.
- [17] X. Peng et al., "Incorporating Reference in Parallel Imaging and Compressed Sensing", Magn. Reson. Med., vol. 73, no. 4, 2014.
- [18] M. T. Bevacqua, L. Crocco, L. Di Donato and T. Isernia, "Microwave Imaging of Nonweak Targets via Compressive Sensing and Virtual Experiments," IEEE Antennas and Wireless Propagation Letters, 14, 2015.
- [19] B. Ouyang et al., "Underwater Laser Serial Imaging Using Compressive Sensing and Digital Mirror Device", Proc. SPIE, vol. 8037, 2011.
- [20] U. Gamber, P. Boesiger and S. Kozerke, "Compressed Sensing in Dynamic MRI," Magnetic Resonance in Medicine, vol. 59, no. 2, 2008.
- [21] M. Lustig, D. Donoho, and J. Pauly, "Rapid MR Imaging with Compressed Sensing and Randomly Under-sampled 3DFT trajectories," Proc Ann Meeting of ISMRM, Seattle, WA, 2006.
- [22] M. Grant and S. Boyd, "CVX: Matlab software for disciplined convex programming", version 2.0 beta. <http://cvxr.com/cvx>, September 2013.
- [23] Ionospheric and Atmospheric Remote Sensing, <https://iono.jpl.nasa.gov/index.html>.
- [24] Ionosphere Monitoring and Prediction Center <https://impc.dlr.de/>.
- [25] Space Weather Prediction Center, National Oceanic And Atmospheric Administration, <https://www.swpc.noaa.gov/>.
- [26] Australian Government Bureau of Meteorology, Space Weather Services <https://www.sws.bom.gov.au/>.
- [27] Global Ionosphere Maps Produced by CODE <http://aiuws.unibe.ch/ionosphere/>.
- [28] U. Sezen, F. Arkan, O. Arkan, O. Uurlu, and A. Sadeghimorad, "Online, Automatic, Nearreal Time Estimation of GPSTEC: IONOLABTEC", Space Weather, 11, 2013.
- [29] H. Nayr, F. Arkan, O. Arkan and C. B. Erol, "Total Electron Content Estimation with RegEst," J. Geophys. Res., 112, A11313, 2007.
- [30] R. Orus, M. Hernandez-Pajares, J.M. Juan, J. Sanz, "Improvement of Global Ionospheric VTEC Maps by Using Kriging Interpolation Technique", J. Atmos. Sol. Terr. Phys., 67, 2005.
- [31] P. Wielgosz, D. Grejner-Brzezinska and I. Kashani, "Regional Ionosphere Mapping with Kriging and Multiquadric Methods," Positioning, Vol. 1 No. 4, 2003.
- [32] S. Schaer, "Mapping and Predicting The Earths Ionosphere Using The Global Positioning System", Ph.D. dissertation, 1999, Astronom. Inst., Univ. of Bern, Bern, Switzerland.
- [33] M. Gurun, K. E. Akdoan and A. Yilmaz, "Regional Ionosphere Mapping By Using Neural Networks," 2007 3rd International Conference on Recent Advances in Space Technologies, 2007.
- [34] I. Sayn, F. Arkan, and O. Arkan, "Regional TEC Mapping with Random Field Priors and Kriging", Radio Sci., 43, RS5012, 2008.
- [35] M. N. Deviren, and F. Arkan, "IONOLAB-MAP: An Automatic Spatial Interpolation Algorithm for Total Electron Content", Turkish Journal of Electrical Engineering & Computer Sciences, 2018.